de Haas–van Alphen effect in the mixed state of $LuNi_2B_2C$: Anisotropy and field dependence of the damping due to superconductivity

T. Isshiki, N. Kimura, and H. Aoki
Department of Physics, Graduate School of Science and Center for Low Temperature Science, Tohoku University, Sendai, Miyagi 980-8578, Japan

T. Terashima and S. Uji
National Institute for Materials Science, Ibaraki 305-0044, Japan

K. Yamauchi
CNR-INFM, CASTI Regional Lab., I-67010 Coppito (L'Aqulia), Italy

H. Harima
Department of Physics, Kobe University, Noda, Kobe 657-8501, Japan

D. Jaiswal-Nagar, S. Ramakrishnan, and A. K. Grover
Department of Condensed Matter Physics and Materials Science, Tata Institute of Fundamental Research, Colaba, Mumbai-400005, India

(Received 25 May 2008; published 30 October 2008)

We report observation of the de Haas-van Alphen oscillations in the mixed state as well as in the normal state of $LuNi_2B_2C$. Two oscillations α and η are observed in the mixed state. In particular, the α oscillation can be studied not only deep in the mixed state as a function of magnetic field but also as a function of field direction. The damping rate of the oscillations due to superconductivity is found to be very anisotropic. For fields far below H_{c2}, the damping behavior is anomalous and cannot be explained only in terms of the superconducting gap. We argue that both the anisotropy of the gap and a disorder of the flux line lattice are responsible for the anisotropic and anomalous behavior of the damping in the mixed state.

DOI: 10.1103/PhysRevB.78.134528 PACS number(s): 74.70.Dd, 74.25.Ha, 74.25.Qt

I. INTRODUCTION

The quantum oscillation in the mixed state of a superconductor was first reported by Graebner and Robbins[1] in $NbSe_2$. After ten years, the discovery of the high-T_c cuprates strongly motivated experimental attempts to observe the quantum oscillations in the mixed state[2,3] because their upper critical fields (H_{c2}'s) are too high to observe the quantum oscillations in the normal state. There are now a number of compounds where the observation of the quantum oscillations in the mixed state has been reported. Although the observation of the quantum oscillations in the mixed state appears to be puzzling, it is now accepted that the quantum oscillation exists in the mixed sate.

In most of the experiments, the quantum oscillation of magnetization, i.e., the de Haas-van Alphen (dHvA) effect, is measured. It is established from the previous experiments that the frequency of the dHvA oscillation in the mixed state is the same as that in the normal state. The effective mass is also the same in the normal state and mixed state, except for those reported for the heavy fermion compounds $CeRu_2$, URu_2Si_2, and UPd_2Al_3.[4] On the other hand, the amplitude of the dHvA oscillation in the mixed state is strongly affected by superconductivity. The additional damping in the mixed state has been studied theoretically as well as experimentally. Most of the theories are appropriate for fields not far from H_{c2} and explain the damping in the mixed state in terms of the superconducting gap.[5–10] However, in many cases, no satisfactory agreement has been obtained between the theoretical predictions and experimental results. Particularly, the field dependence of the dHvA oscillations cannot be explained in terms of the gap. There are also some experimental results which suggest that a disorder of the flux line lattice is another source to deteriorate the dHvA oscillations in the mixed state.[9,11] Since in the proposed theories an average or an assumption is made for the spatial variation in the gap, this effect may not be suitably taken into account. At the present stage, the understanding of the dHvA oscillations in the mixed state is far from complete experimentally as well as theoretically.

We may improve our understanding of the problems mentioned above to a large extent if we can observe the dHvA oscillations in the mixed state for the following cases: (1) The Fermi surface has an anisotropic gap or the gap is different depending on the Fermi surface: (2) The flux line lattice changes depending on the field strength or field direction. In these respects, borocarbide superconductors YNi_2B_2C and $LuNi_2B_2C$ are very suitable candidates for the study of the dHvA oscillations in the mixed state.

YNi_2B_2C and $LuNi_2B_2C$ are nonmagnetic superconductors whose T_c values are 15.6 K and 16.2 K, respectively.[12] These two compounds have interesting features in common as follows. Various measurements[13–19] indicate that the superconducting gap is anisotropic. Particularly angle-resolved thermal transport[15] and heat-capacity measurements in YNi_2B_2C (Ref. 16) and in $LuNi_2B_2C$ (Ref. 17) suggest that

 ©2008 The American Physical Society

the gap function has point nodes in the ⟨100⟩ directions. It is also theoretically predicted that the superconducting order parameter is anisotropic and has point nodes in the (001) plane.[20,21] On the other hand, point contact spectroscopy[18] and specific-heat measurements[19] in YNi_2B_2C indicate that the results can be also explained by a multigap model.

They have also very intriguing flux line lattice properties. Neutron scattering, scanning tunnel spectroscopy, and other measurements on YNi_2B_2C or $LuNi_2B_2C$ have revealed that these compounds could exhibit flux line lattice transitions as a function of field, field direction, and temperature.[17,22–28] For the fields parallel to the [001] direction, a hexagonal flux lattice is formed in low fields below about 0.1 T in YNi_2B_2C or 0.02–0.05 T in $LuNi_2B_2C$, but at higher fields it changes to a square lattice. With increasing field above 1–2 T, a disorder in the lattice develops[24,25] and finally becomes amorphous, leading to the peak effect. Besides the peak effect in the field region just below H_{c2}, another anomaly in the critical current density J_c is sometimes observed deep in the mixed state.[29,30] This anomaly is referred as the second magnetization peak or the multimagnetization peak, but its origin has not been clarified yet. In fields close to H_{c2}, the hexagonal flux lattice is likely to recover.[27,28] For fields parallel to ⟨100⟩ and ⟨110⟩ directions, the transition fields from hexagonal to square lattice increase to about 1–2 T.[17,25]

So far, several dHvA effect studies in the mixed state of YNi_2B_2C have been reported.[31–36] But most of the studies were performed with fields parallel to the [001] direction or directions near the [001] direction and also for a single Fermi surface except for the one by Heinecke and Winzer.[31] They observed two different dHvA oscillations both in the normal and mixed states with fields parallel to the [001] direction but found no additional effect on the signal amplitudes due to superconductivity. On the other hand, the other studies report significant effects of superconductivity on the dHvA signal. For $LuNi_2B_2C$, the dHvA effect in the mixed state was recently reported but the observation is possible also in limited field directions around the [001] direction.[37] Therefore, there is no sufficient experimental information reported to discuss about the effects of the superconducting gap and the disorder of the flux line lattice. In this paper we report observation of the dHvA oscillations of $LuNi_2B_2C$ deep in the mixed state. Moreover, we report observation of the dHvA oscillations from a single Fermi surface for various field directions, including those along three high-symmetry directions [001], [100], and [110]. We also report observation of another dHvA oscillation from a different Fermi surface whose character is very different from the former one. We will discuss the implications of the present results in conjunction with the reports on the anisotropic gap and the disorder in the flux line lattice.

II. METHODS

A. Experimental methods

The single crystals of $LuNi_2B_2C$ were grown by the flux method using Ni_2B as flux.[38] Two samples, A and C, are used in the present experiment. The names of the samples correspond to those in the magnetization measurements performed on the same samples.[30] They have platelet shapes with the [001] axis normal to the plane of the platelet. The data presented in this paper were collected in sample C if not otherwise stated. The dHvA effect and ac susceptibility measurements were performed in top loading dilution refrigerators under magnetic fields up to 17 T. We employed the field modulation method to detect the dHvA oscillations. The modulation frequency and field were 67 Hz and 10 mT, respectively, if not otherwise stated. The field dependence of the dHvA amplitude in the mixed state was measured with decreasing field from the normal state at 100 mK except for the case of effective mass measurement.

B. dHvA effect in the mixed state

The oscillatory magnetization of the dHvA effect $\tilde{M}$ is given by the following Lifshitz and Kosevich (LK) formula:[39]

$$\tilde{M} \propto \frac{\beta F B^{1/2} V}{(A'')^{1/2}} \sum_{p=1}^{\infty} \frac{R_T R_D R_S}{p^{3/2}} \sin\left[2\pi p\left(\frac{F}{B} - \gamma\right) \pm \frac{\pi}{4}\right]. \quad (1)$$

Here, B is the magnetic field and V is the volume of the sample. F is the frequency of the oscillation given by

$$F = \frac{\hbar}{2\pi e} A. \quad (2)$$

A is the extremal cross-sectional area of the Fermi surface perpendicular to the applied field and β is given by

$$\beta = \frac{e\hbar}{m^*}, \quad (3)$$

where m^* is the effective mass. The oscillation consists of the fundamental frequency oscillation ($p=1$) and harmonic frequency oscillations ($p>1$). γ in the sine function is thought to be 1/2 in normal metals. $\pm$ sign in the cosine function indicates that the $-(+)$ corresponds to the maximal (minimal) cross-sectional area. A'' is the curvature factor given by

$$A'' = \left|\frac{\partial^2 A}{\partial k_H^2}\right|. \quad (4)$$

Here, k_H is the parallel component of the crystal momentum $\vec{k}$ to the applied magnetic field. R_T is the temperature damping factor given by

$$R_T = \frac{2\pi^2 p k_B T/\beta B}{\sinh(2\pi^2 p k_B T/\beta B)} \quad (5)$$

and denotes how the signal amplitude changes with temperature. R_D is the Dingle damping factor given by

$$R_D = \exp(-2\pi^2 p k_B T_D/\beta B) \quad (6)$$

and denotes reduction of the signal amplitude by scattering. Here, T_D is the Dingle temperature, which is inversely proportional to the relaxation life time τ of the electron,

$$T_D = \hbar/2\pi k_B \tau. \quad (7)$$

If we plot the reduced signal amplitude $\ln(Amp\ B^{-1/2}/R_T)$ against $1/B$ in the normal state, we obtain a straight line and

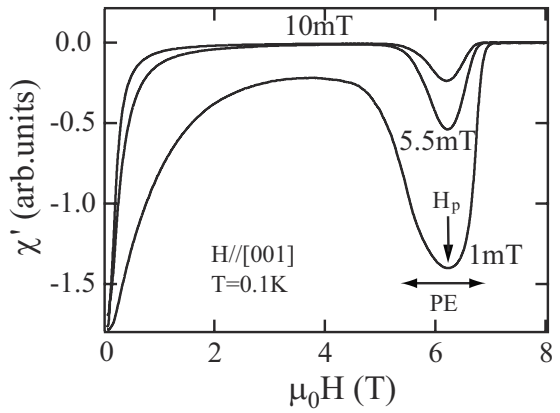

FIG. 1. ac susceptibilities as a function of applied field at 100 mK for modulation fields 1, 5.5, 10 mT. H_p is the peak field in the peak effect (PE) region.

the value of the Dingle temperature from the slope. R_S is the spin splitting factor given by

$$R_S = \cos\left(\frac{1}{2} p \pi g m_b / m_0\right), \tag{8}$$

where m_0 and m_b are the electron rest mass and the band mass, respectively. This factor arises from the Zeeman splitting of the Landau levels. m_b may be replaced by m^* in a strongly correlated electron system.[40] When we use the field modulation method for detection, the amplitude detected by using the kth harmonic of the modulation frequency is multiplied by the following Bessel factor:

$$J_k\left(\frac{2\pi F b}{B^2}\right). \tag{9}$$

Here, J_k is the Bessel function and b is the modulation-field amplitude. Because of this factor, an appropriate modulation-field amplitude should be chosen depending on the dHvA frequency and the magnetic field.

We assume that an additional damping factor R_{DS} is multiplied in the mixed state. In addition to the mechanisms mentioned in Sec. I, there are other mechanisms which could affect the amplitude of the dHvA oscillation. The field inhomogeneity in the mixed state was carefully discussed by Janssen *et al.*[41] This effect is found to give negligible effect on the damping of the dHvA oscillation. The influence of the pinning effect was also discussed by Janssen *et al.*,[41] using the Bean's critical state model. It is demonstrated that when $b \gg B^*$, the influence of the pinning is negligible.[41] Here, $B^* = (1/2)\mu_0 J_c a$ and a is the flux line lattice parameter, respectively. We have performed magnetization studies on the same crystals to estimate J_c in the temperature range between 10 and 2 K.[42] It is found that $B^* \sim 1$ mT at 2 K in the range above 2 T, except for the region where the peak effect is observed. It is also found that J_c values change only by a factor of 1.5 from 6.5 to 2 K; therefore, it is likely that J_c values do not change considerably from 2 to 0.1 K. In fact, we can confirm that the condition $b \gg B^*$ is realized at 0.1 K from the ac susceptibility measurements as shown in Fig. 1. For the modulation fields 5.5 and 10 mT, the value of the ac susceptibility below the onset field of the peak effect and down to about 2.5 T is nearly the same as that in the normal state. However, for the small modulation field of 1 mT, the ac shielding response is substantial, indicating the survival of finite pinning with smaller ac modulation. These observations imply that for the sufficiently large ac modulation field used in the dHvA measurements, the flux array can move according to the modulation field, and the pinning effect on the measured signal amplitude is not significant.

We have compared our results also with predictions of the proposed theories.[5–8,10] None of the predictions agree with our experimental results. We display only the prediction by Maki[5] together with our experimental results. A careful comparison with various theoretical predictions in the cases of V_3Si and $NbSe_2$ was given in the work of Janssen *et al.*[41] In Maki's theory the additional damping factor is given by

$$R_{DS} = \exp\left[-\pi^{3/2}\left(\frac{\Delta m_b}{\hbar e B}\right)^2 \left(\frac{B}{F}\right)^{1/2}\right], \tag{10}$$

where Δ is the gap function, which is averaged over the orbit, and its field dependence is assumed to be

$$\Delta(H) = \Delta(0)\sqrt{1 - \frac{H}{H_{c2}}}. \tag{11}$$

For Eq. (11), we use the upper critical field H_{C2}, which is determined from the ac susceptibility measurement. Our values of H_{C2}'s agree well with those of some previous reports[43–45] but are smaller than those of the other reports.[37,46,47] The value of H_{C2} may depend on the sample quality, as well as on the method of measurement or on how we define the value of H_{C2}. We assume that the superconducting gap energy is 2.46 meV, which corresponds to the value predicted by Bardeen-Cooper-Schrieffer (BCS) theory for weak coupling with $T_c = 16.2$ K. This value is close to 2.2 meV determined by the scanning tunneling microscopy measurement.[23]

C. Band-structure calculations

In order to assign the measured dHvA frequency branches to the Fermi surfaces, we have performed a band-structure calculation within the local density approximation (LDA) in the density-functional framework using the full potential linearized augmented plane-wave (FLAPW) formalism.[48] We used TSPACE and KANSAI-99 program codes for this calculation. In the D_{4h}^{17} crystal structure, the room-temperature lattice constants $a = 3.464$ Å and $c = 10.631$ Å and an internal parameter of B atom at the 4e site as 0.362 are used.[49] Muffin-tin radii are set as $0.4707a$, $0.3358a$, $0.2010a$, and $0.2010a$ for Lu, Ni, B, and C sites, respectively. The linearized augmented plane-wave (LAPW) basis functions are truncated at $|\mathbf{k}+\mathbf{G}_i| = 4.01 \times 2\pi/a$, corresponding to 405 LAPW functions at Γ point. The sampling 369 k points (divided by 16, 16 and 8) are uniformly distributed in the irreducible 1/16th of the body-centered-tetragonal Brillouin zone. The "semicore" states of Lu-5p and Ni-3p electrons are treated as valence states by using a second energy window. The scalar relativistic effects are taken into account for

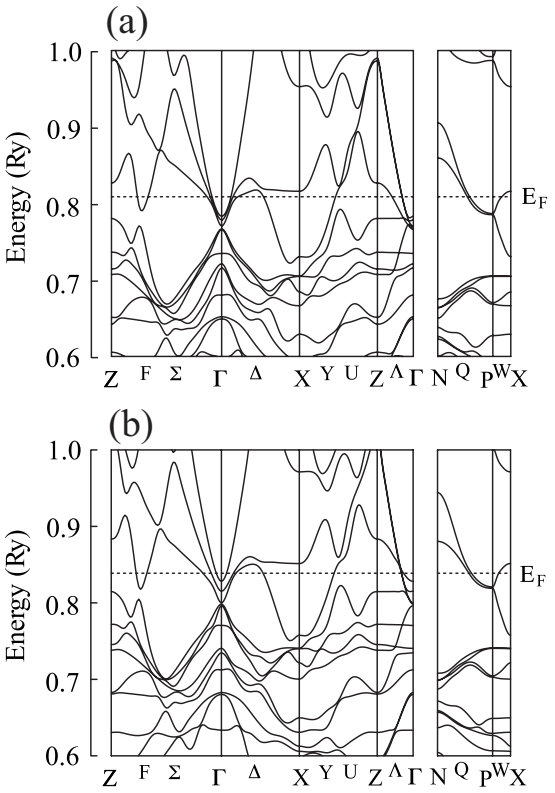

FIG. 2. Band structure of $LuNi_2B_2C$: (a) LDA result, (b) Lu-*d*, and Ni-*d* energy levels are shifted upward by 0.11 and 0.05 Ry from the LDA result (see text). E_F denotes the Fermi energy.

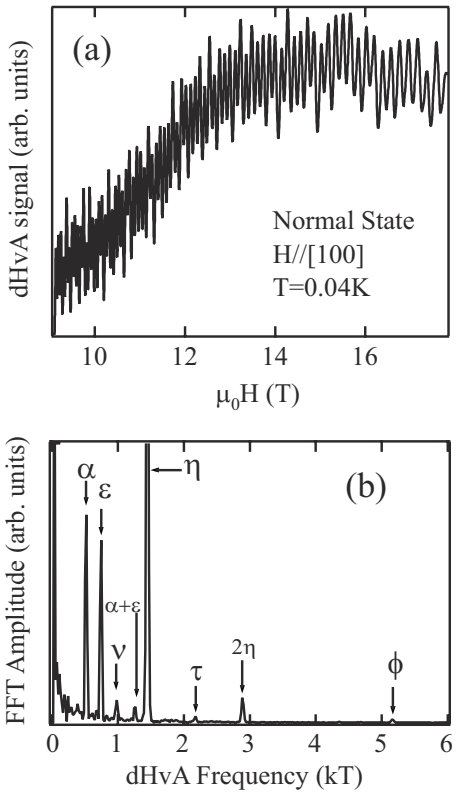

FIG. 3. (a) dHvA signal in the normal state with fields parallel to the [100] direction at 40 mK. (b) Fourier spectrum of the signal.

all electrons, and the spin-orbit interactions are included self-consistently for all valence electrons inside the muffin-tin spheres as in a second variational procedure. These methods of calculations are the same as the previous calculations performed by some of us.[50]

The previous study for YNi_2B_2C (Ref. 51) has shown that the calculated result with the LDA potential gives the disagreement with the experimental results so that the calculated Y-4*d* and Ni-3*d* levels are shifted upward from the LDA levels by 0.11 Ry and 0.05 Ry, respectively, in order to reproduce the experimentally observed Fermi surfaces. In this calculation of $LuNi_2B_2C$, we have found that the same modification is necessary to obtain the Fermi surfaces, which describe the observed dHvA oscillations successfully. Figures 2(a) and 2(b) show the resulted band structure of the LDA calculation and that with the modification where Lu-4*d* and Ni-3*d* levels are shifted upward from the LDA levels by 0.11 Ry and 0.05 Ry, respectively. Our LDA band structure looks similar to the recent theoretical study within LDA reported by Bergk *et al.*[52] except the effect of the spin-orbit interaction taken into account in our calculation so that the degenerated energy levels are left in some points. As shown in Fig. 2, three bands (33rd, 34th, and 35th) cut the Fermi energy and bring the complicated Fermi surfaces. With our modification of the energy levels, the 35th band is significantly shifted above around the Γ point, and consequently, the shape of the corresponding Fermi surface [indicated by α in Fig. 6(c)] becomes slim. The comparison of the calculated Fermi surfaces with the experimental result will be discussed in Sec. III.

III. RESULTS AND DISCUSSIONS

A. Normal state

In this subsection, we report the dHvA effect results in the normal state and compare them with the band-structure calculations. Figures 3(a) and 3(b) show the dHvA signal with fields along the [100] direction and its Fourier spectrum. Eight frequency branches α, β, γ, ϵ, η, ϕ, ν, and τ are observed and their angular dependences are plotted in Fig. 4.

Except for ϕ, ν, and τ, we find the similar frequency branches in YNi_2B_2C and use the same notation for the corresponding frequency branches.[32,53] The α oscillation can be observed for all the field directions studied, indicating that it arises from an ellipsoidal Fermi surface. The η oscillation could not be observed for the field directions near the [001] direction probably because the signal amplitude was weak, but not because the closed orbit does not exist. Other frequency branches could be observed in the limited field directions.

Figures 5 and 6 show the angular dependence of the dHvA frequencies and the Fermi surfaces derived from the band-structure calculations with the energy modification, respectively. The electron orbits corresponding to the dHvA frequency branches in Fig. 5 are shown in Fig. 6. We assigned the α, γ, η, and ϕ branches as the observed dHvA branches, whereas the *e*, *f*, and *j* branches have not been observed. Compared with Fig. 4, the angular dependence of the α, γ, η, and ϕ branches shows a substantially good correspondence with the experimental result. For α, η, and ϕ branches, the mass enhancement factor λ is calculated by the

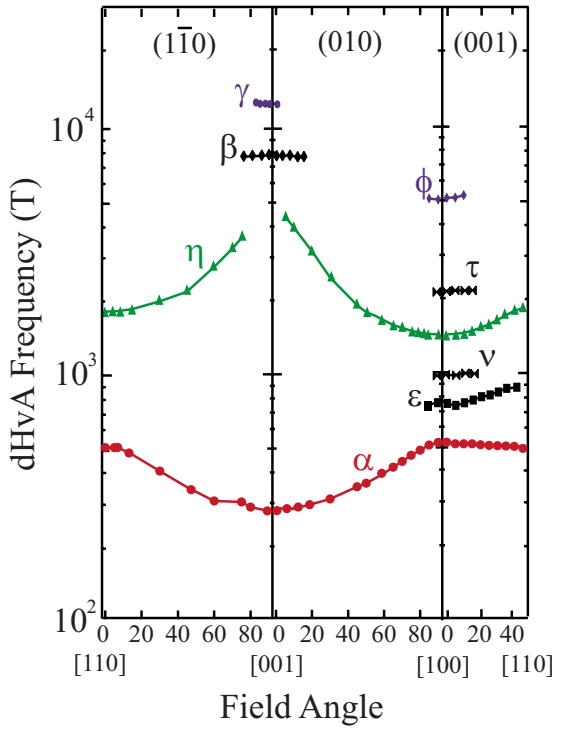

FIG. 4. (Color online) Angular dependence of the experimental dHvA frequencies.

comparison of the calculated cyclotron mass (band mass) m_b and the measured effective mass m^*, using the definition as $m^*=(1+\lambda)m_b$. Table I shows the measured dHvA frequency,

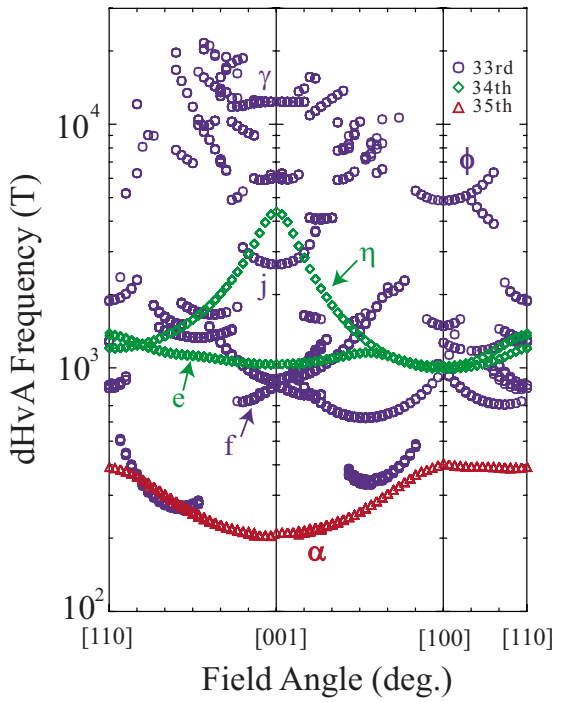

FIG. 5. (Color online) Angular dependence of the dHvA frequencies obtained by the band-structure calculation. The symbols of ○(blue), ◇(green), and △(red) indicate the frequencies originating from the 33rd, 34th, and 35th band, respectively.

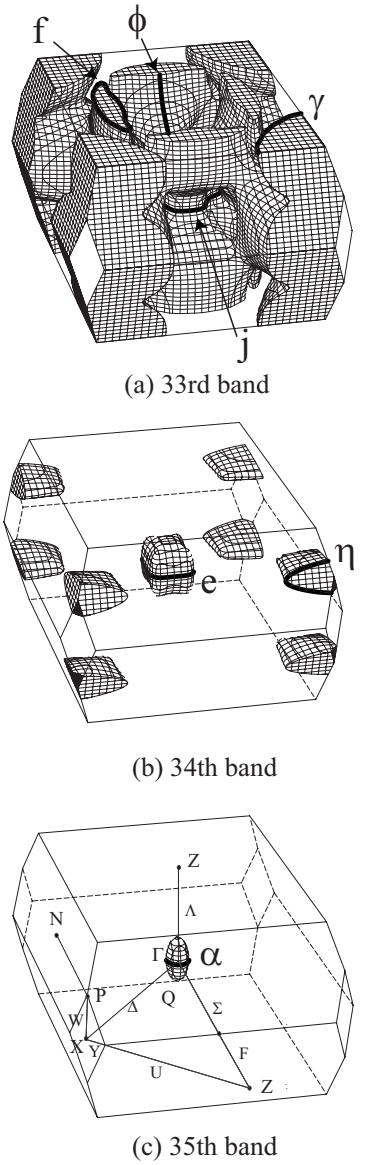

FIG. 6. Fermi surfaces derived from (a) 33rd, (b) 34th, and (c) 35th band in the first bct Brillouin zone, obtained by the band-structure calculation. The shaded parts are occupied by the electron. The electron orbits corresponding to the dHvA branches (see Fig. 5) are visualized by thicker lines.

the effective mass, the band mass, the mass enhancement factor, and the Dingle temperature in the normal state for the fields parallel to the high-symmetry directions [001], [100], and [110].

Recently, Bergk *et al.*[52] reported the dHvA effect experiment and the band-structure calculation in the normal state of $LuNi_2B_2C$. They employed a magnetic torque method with a capacitive cantilever torquemeter to detect the dHvA oscillations and utilize the high magnetic fields up to 32 T. We could not detect the $F_{\sigma 1}$ and F_{ϵ} branches reported by them, while they do not report the τ branch. There is also a significant difference in the results of the band-structure calculations for the α branch. As mentioned before, the energy modification significantly changes the shape of the α Fermi surface. The spherical Fermi surface, which is obtained

TABLE I. dHvA frequency F, effective mass m^*, and band mass m_b in units of electron rest mass m_0, mass enhancement factor λ, and the Dingle temperature $T_D(K)$ in the normal state, for the high-symmetry directions, [001], [100], and [110].

Direction		F(T)	$m^*(m_0)$	$m_b(m_0)$	λ	T_D(K)
[001]	α	281	0.30	0.20	0.50	1.98
	β	7780	1.53			
	γ	12600		2.11		
	η			2.11		
[100]	α	521	0.49	0.36	0.36	1.98
	ϵ	770	0.89			
	ν	980	0.41			
	η	1450	1.30	0.43	2.02	2.20
	ϕ	5140	1.54	0.58	1.66	
	τ	2180	1.44			
[110]	α	505	0.43	0.37	0.16	3.25
	η	1840				

within LDA (comparable with the one by Bergk *et al.*), is reduced in the volume and whose shape becomes more ellipsoidal along the k_z axis after the modification, in agreement with the observed dHvA branch. Since the cyclotron mass is sensitive to both the shape and the size of the Fermi surface, the value of λ and its anisotropy claimed by Berk *et al.*, i.e., 0.8 ([110])-0.3 ([001]), changes to 0.16 ([110])-0.5 ([001]).

In the next subsection, we focus on the α and η branches, whose oscillations are also observed in the mixed state as reported. The α branch originates from the ellipsoidal electron Fermi surface of the 35th band, centered at the Γ point; η branch originates from the closed electron Fermi surface of the 34th band around the P point (cfr. Fig. 6).

B. Mixed state

We have successfully observed the α oscillation in the mixed state not only for the field parallel to [001], but also for fields parallel to [100] and [110] directions and the directions in between these high-symmetry directions. Figure 7 shows the α oscillation with field parallel to the [001] direction. Except for the peak effect region, very clear signal can be observed down to very low fields, $H/H_{c2}=0.22$. In addition to the α oscillation, the η oscillation can be observed in the mixed state for the field directions near [100]. In Figs. 8(a) and 8(b), we show the dHvA oscillations and Fourier spectra in the normal state and mixed state to demonstrate that the η oscillation survives in the mixed state. The frequencies, as well as the effective masses, are found to be the same in the normal state and mixed state for both the α and η oscillations.

Figure 9 shows the Dingle plot of the α oscillations with fields parallel to the [001] direction for the two samples, A and C. We determined the amplitude of the α oscillation from peak to peak amplitude after extracting only the fundamental frequency of α by using a digital filter. We define the field value at the midpoint between the positions of two peaks as the field value for the peak to peak amplitude. Different amplitudes of the modulation field, i.e., 10 and 4 mT, are used in the high field region and low field region, respectively, to optimize the detection condition of Eq. (9). In the middle field region, both the modulation-field amplitudes are used to confirm that both of them give the same Dingle plot, as shown in Fig. 10. The signal in the peak effect region is strongly damped and is difficult to measure by the large signal shift due to the peak effect. Therefore, we omit data points from the Dingle plots in the peak effect region in figures from Figs. 9–15. The Dingle plots of the two samples are similar to each other, as shown in Fig. 9. They have nearly the same slopes as those of the normal state in fields just below the peak effect region. With further decrease in field, the slope becomes steeper above about $1/(\mu_0 H)=0.25$ T^{-1} (or below about $\mu_0 H=4$ T) in sample C and above about $1/(\mu_0 H)=0.30$ T^{-1} (or below about $\mu_0 H=3.3$ T) in sample A. Then, above about $1/(\mu_0 H)=0.45$ T^{-1} [or below about $\mu_0 H=2.2$ T ($H=0.31H_{c2}$)], the slope becomes again as small as that of the normal state, making a kink structure on the plot (see Fig. 9). The slopes and the positions of the kink are slightly different between the two samples, and the kink structure is less obvious in sample A. In Fig. 11, we show the Dingle plots of the α oscillation in the $(1\bar{1}0)$ plane. The position of the kink moves to higher fields with tilting the field direction from [001] to [110] in the $(1\bar{1}0)$ plane. This behavior is also observed in the (010) plane. However, the lowest field, where the signal can be observed clearly, increases more rapidly with the tilting angle, and therefore, the kink structure cannot be observed clearly for the directions with the tilting angle more than 45 degrees from the [001] direction. The origin of the kink structure is discussed later.

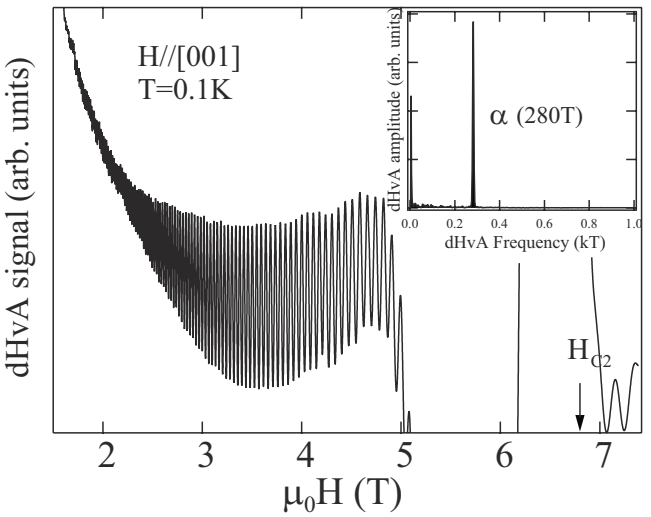

FIG. 7. α oscillation in the mixed state and its Fourier spectrum (inset) with fields parallel to the [001] direction. The signal in the peak effect region is not displayed in the figure.

Figures 12(a), 12(b), and 12(c) show the damping factor R_{DS} of the α oscillations as a function of magnetic field for the field directions parallel to [001], [110], and [100], respectively. It is noted that the range of abscissa is much larger in panel (a) than in panels (b) and (c) in Fig. 12. The larger scatter of the data points of [100] and [110] directions is due

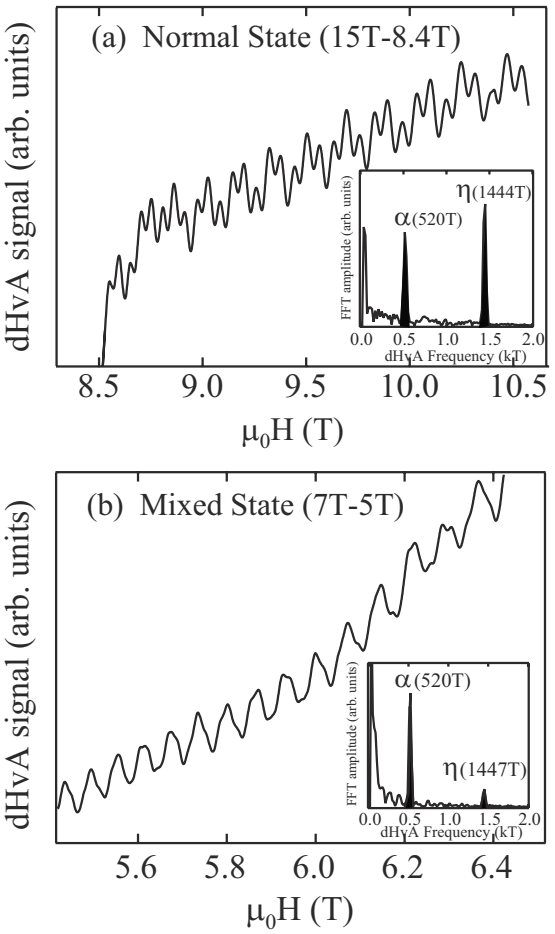

FIG. 8. dHvA oscillations and Fourier spectra (a) in the normal state and (b) in the mixed state for fields parallel to the [100] direction. The η oscillation, as well as the α oscillation, survives in the mixed state.

to the smaller signal amplitudes and is not directly related with the damping rate. For fields along the [001] direction, the curvature factor and the effective mass are smaller than those with fields along the ⟨100⟩ and ⟨110⟩ directions and give rise to a larger signal amplitude [see Eqs. (1)–(5)]. We also include the field dependence of the dHvA amplitude according to the theory of Maki.[5] We use the band masses to calculate R_{DS}.[41] The damping behavior of the signal amplitude is very different from the theoretical prediction and does not agree with any other theoretical predictions. The damping behavior also depends on the crystal direction: The amplitude in the field range just below H_{C2} is larger than the theoretical value for [001] and [110] and is smaller than that for [100]. When the effective mass is used instead of the band mass to calculate R_{DS}, the theoretical damping rate becomes larger than that shown in the figure. However, the following qualitative features remain the same. For the [001] direction, the theoretical curve crosses the experimental curve. For the [110] direction the theoretical curve lies below the experimental curve, while for the [100] direction the theoretical curve lies above the experimental curve.

In Figs. 13 and 14, we plot R_{DS} in the (001) plane and in the (010) plane, respectively. With tilting the field direction

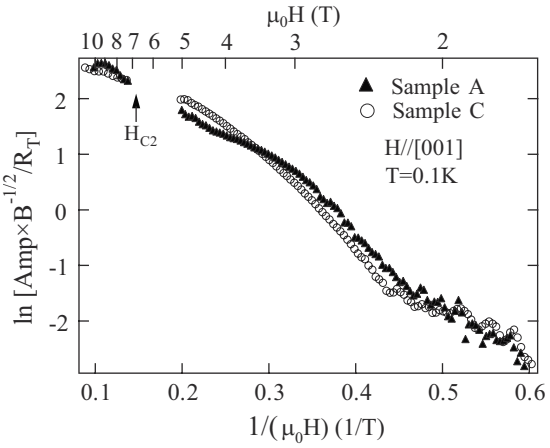

FIG. 9. Dingle plots of the α oscillations in samples A and C. The data points in the peak effect region are not displayed. H_{c2} values at 0.1 K of the samples A and C are 6.81 T and 6.74 T, respectively.

from [110] to [100] and from [001] to [100], the damping rate monotonously increases with tilting angle. As noted from Fig. 11, it also increases with the tilting from [001] to [110]. These results indicate that the damping is least for the fields parallel to [001] and largest for [100], and that there is no other field direction where the damping rate becomes maximum or minimum. If the superconducting gap is solely responsible for the damping of the dHvA signal, these results indicate that the superconducting order parameter is anisotropic.

Figure 15 shows the additional damping factor R_{DS} of the η oscillation as a function of magnetic field. Since the signal amplitude is weak, the amplitude is obtained by Fourier analysis over a certain range of magnetic field, which is shown as the horizontal error bar. For the field range just below the peak effect region, the signal amplitude is larger than the theoretical value. This behavior is different from that of the α oscillation for the fields parallel to the [100] direction in Fig. 12(c).

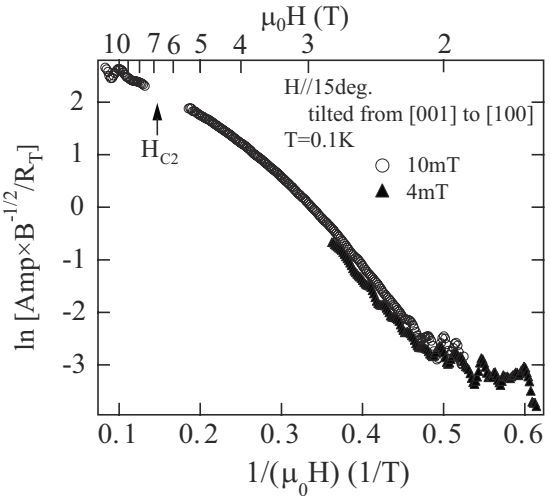

FIG. 10. Dingle plots of the α oscillations detected in sample C by using two different modulation-field amplitudes 10 and 4 mT.

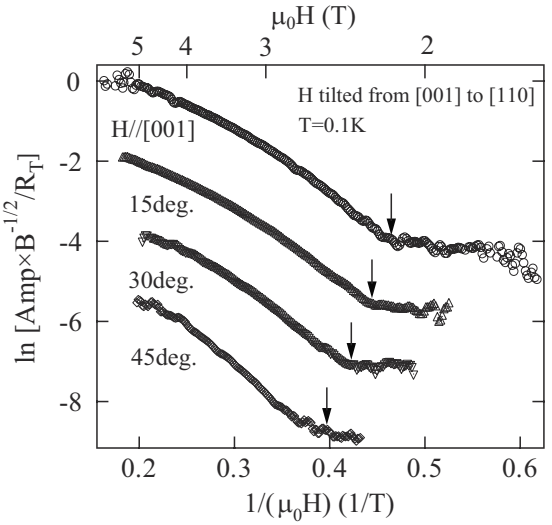

FIG. 11. Dingle plots of the α oscillations in the mixed state for fields in the $(1\bar{1}0)$ plane. Data points at each angle are shifted vertically for clarity. The arrows indicate the positions of the kinks.

To summarize interesting observations in the mixed state briefly:

(a) We have observed the dHvA oscillations which arise from the two different Fermi surfaces. For the Fermi surface of α, the signal can be observed for various field directions, including those parallel to three high-symmetry directions.

(b) The damping rate due to superconductivity strongly depends on the field direction and possibly on the Fermi surface.

(c) The damping rate critically depends on magnetic-field strength, and the resultant kink structure is observed.

First, we discuss observations (a) and (b). As mentioned above, the angular dependence of R_{DS} indicates that $LuNi_2B_2C$ is likely to have an anisotropic superconducting gap. Previous experiments[15,16] point out that there are point nodes of the gap in the ⟨100⟩ directions in the (001) plane. However, a recent calculation using a more realistic electronic structure[54] shows that the experimental results can be explained by assuming that the point nodes reside in the ⟨110⟩ direction rather than in the ⟨100⟩ direction. When the field is parallel to the ⟨001⟩ or ⟨100⟩ direction, the orbit includes four and two positions of the point node, respectively. On the other hand, the orbit does not include it when the field is parallel to the ⟨100⟩ direction. If the point node significantly affects the amplitude of the dHvA oscillation, the damping factor will be largest for the field parallel to the ⟨100⟩ direction. Therefore, the present results are consistent with the previous experiments. On the other hand, it is pointed out that the point node does not significantly increase the signal amplitude.[10] Although the present results strongly suggest that the gap is anisotropic on the α Fermi surface, it might not be certain that point nodes exist on the α Fermi surface.

The η oscillation can be observed in the mixed state only with fields parallel to [100]. We suspect that this anisotropy of the signal amplitude in the mixed state does not arise from an anisotropic rate of the damping due to superconductivity, but arises from the anisotropic amplitude in the normal state.

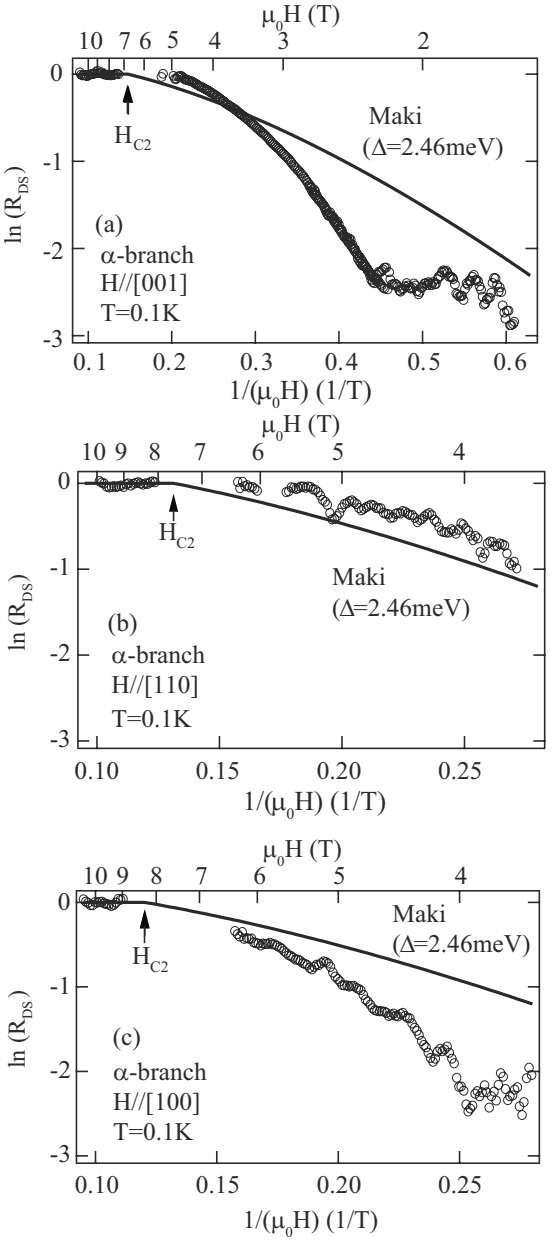

FIG. 12. Additional damping factor R_{DS} due to superconductivity as a function of inverse field for fields parallel to the (a) [001], (b) [110], and (c) [100] directions. The solid curves are the theoretical values by Maki (Ref. 5) using 2.46 meV as the gap value. Note that the range of the abscissa is much larger in panel (a) than in panels (b) and (c).

As noted from the dHvA effect in the normal state (Fig. 4 and Table I), the values of the curvature factor [Eq. (4)] and effective mass [Eq. (5)] of η oscillation are the smallest in the [100] direction. Accordingly it has the largest signal amplitude for the fields parallel to [100]. On the other hand, it has smaller amplitudes for the fields in other high-symmetry directions, and in particular for fields in the [001] direction it could not be observed even in the normal state. Therefore, the additional damping due to superconductivity may have suppressed the signal amplitude under noise level except for the [100] direction. The different damping behaviors are observed between the Fermi surfaces of α and η with fields in

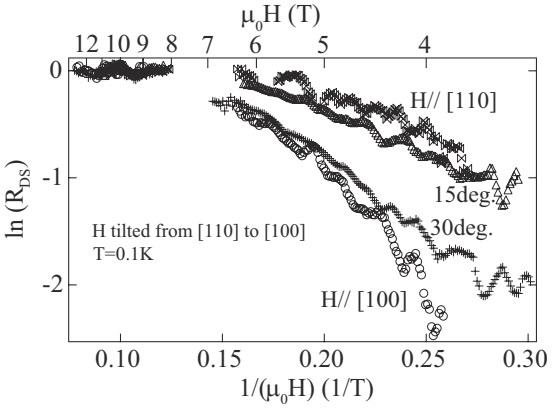

FIG. 13. Angular dependence of the additional damping factor R_{DS} as a function of inverse field in the (001) plane.

the [100] direction, i.e., the damping rate is larger than the theoretical values for α, while it is smaller for η. Since the α and η oscillations arise from the different bands, the characters of the wave functions such as s-, p-, and d-like are different at the Fermi surface. It is also noted from Table I that the mass enhancements or the strengths of electron-phonon interaction are considerably different between the two oscillations. Therefore, the difference in the damping behaviors could arise from the different superconducting gap.

Now we discuss observation (c). The field dependence of R_{DS} cannot be explained by the theoretical prediction, which assumes the field dependence of the gap given by Eq. (11). Any realistic model of the field dependence of the gap would not explain the field dependence, which shows the kink behavior. On the other hand, the kink structure of the Dingle plot can be also observed when the dHvA oscillations form a beat structure.[40,55,56] In this case, the kink position corresponds to the minimum position of the beat structure. The beat structure arises when (i) there is a warping of the Fermi surface, i.e., there are maximum and minimum extremal cross-sectional areas perpendicular to the applied field direction, (ii) the sample consists of two crystals whose orientations differ slightly from each other, and (iii) the effective

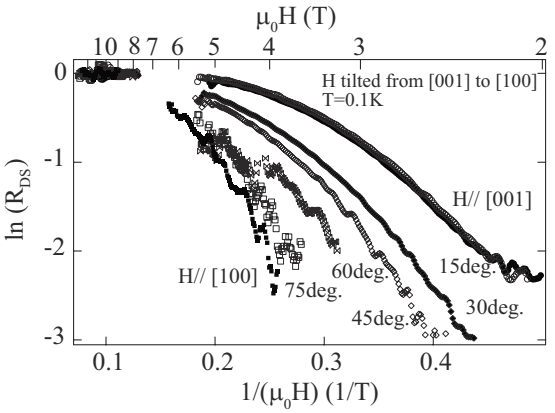

FIG. 14. Angular dependence of the additional damping factor R_{DS} as a function of inverse field in the (010) plane. The field is tilted from [001] to [100]. The data for H//[100] is the same as those plotted in Fig. 13.

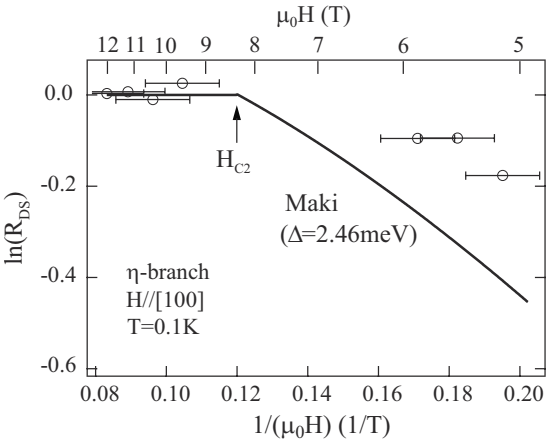

FIG. 15. Additional Dingle factor due to superconductivity for the η oscillation with fields parallel to the [100] direction. The horizontal error bars denote the field range used for the Fourier analysis to obtain the signal amplitudes. The solid curves is the theoretical value by Maki (Ref. 5) using 2.46 meV as the gap value.

masses of the up and down spin oscillations are different and depend on magnetic field. Case (iii) is often observed in the strongly correlated f-electron compounds related with the spin splitting factor [Eq. (8)][40] and is not relevant in the present case. In cases (i) and (ii), the two different oscillations arising from two extremal cross-sectional areas or from a bicrystal structure interfere to form the beat structure. Simple mathematics shows that from the position of the kink we can estimate $\Delta F/F$, where F is the average of the frequencies of the two oscillations and ΔF is the difference. When fields are applied parallel to the [001] direction, $\Delta F/F$ is about 1/173 for the case of the warping, and 1/260 for the case of bicrystal structure. With tilting angle by 45 degrees from [001] toward [110], the $\Delta F/F$ slightly decreases to 1/183 for the case of warping and to 1/274 for the case of bicrystal structure.

If the two frequencies arise from the maximal and minimal orbits on the Fermi surface, the $\Delta F/F$ should decrease rapidly with tilting angle. Moreover, the position and shape of the kink structure should be the same for all samples. As mentioned above, however, the slopes and the positions of the kink are slightly different between the two samples A and C, and the kink structure is less obvious in sample A. It is also difficult to imagine a Fermi surface shape which can give the angular dependence of the kink position in Fig. 11, and at the same time that of the α frequency in Fig. 4. On the other hand, if the two frequencies arise from the bicrystal structure, then the position of the beat minimum depends on the relative difference of the orientations of the two crystals with respect to the field direction, and the relative amplitudes at the minimum and maximum positions of the beat depend on the volumes of the two crystals. Since the kink positions of the two samples A and C are nearly the same, this indicates that the relative difference in the orientations of the two crystals with respect to the applied field direction is almost exactly the same. This is very unlikely. Moreover, the beat structure should be observed for other oscillations like η if the beat structure arises from a bicrystal structure. Therefore, the kink structure or the field dependence of the damping

factor is not likely to be due to the beat structure.

The present observations can be compared with those reported for YNi_2B_2C. Goll *et al.*[33] reported the observation of the α oscillation down to fields of about 4 T ($H/H_{c2} \approx 0.4$ with $\mu_0 H_{c2}=10.5$ T) using a sample grown by a flux method, and using a torque method for the detection of the dHvA oscillation. Their observation is for the fields 14 degrees off from the [001] axis in the (110) plane. Terashima *et al.*[34] observed the α oscillation down to 2 T ($H/H_{c2} \approx 0.23$ with $\mu_0 H_{c2}=8.8$ T) using a sample grown by a floating-zone method, and using the field modulation method. Although the detection method and the sample growth method are different, they give similar results as long as the signal is observed. The signal amplitude in the peak effect region decreases considerably than that in the normal state. Since the signal detected by the field modulation method is damped by the pinning effect, the damping of the signal in the peak effect region is larger in the result by Terashima *et al.*[34] than that by Goll *et al.*[33] However, there is also the significant damping of the signal in the result by Goll *et al.*[33] This observation implies that the disorder of the flux line lattice considerably deteriorates the dHvA signal. Below the peak effect region, i.e., above $1/(\mu_0 H)=0.2$ T^{-1} (or below about $\mu_0 H=5$ T), the damping rate becomes smaller and the slope of the Dingle plot is comparable to that in the normal state in the both results. In the results by Terashima *et al.*,[34] the damping rate becomes slightly larger above $1/(\mu_0 H)=0.32$ T^{-1} (or below about $\mu_0 H=3.1$ T), and then again the damping rate becomes as small as that of the normal state above about $1/(\mu_0 H)=0.38$ T^{-1} (or below about $\mu_0 H=2.6$ T), making a small kink structure in the Dingle plot around 2.6 T($H/H_{c2}=0.30$). The overall behavior of the Dingle plot is similar to that of sample A. These observations indicate that it is likely that the kink structures observed in YNi_2B_2C and $LuNi_2B_2C$ have the same origin.

We discuss a disorder of flux line lattice as a possible mechanism for observation (c). If we extend the slope of the Dingle plot in Fig. 9 just below the peak effect region to the lower field region, the slope meets the data points approximately around $1/(\mu_0 H)=0.6$ T^{-1} or $\mu_0 H=1.7$ T. This observation suggests that the damping rate increases around $1/(\mu_0 H)=0.45$ T^{-1} or around $\mu_0 H=2.2$ T ($H/H_{c2}=0.31$). The pinning effect and the resultant disorder in flux line lattice are possible mechanisms for the damping. However, as noted in Fig. 1, the influence of the pinning effect is negligible under the sufficiently large modulation field at lower fields below the peak effect region. Moreover, the above damping behavior does not correlate with the strength of the pinning effect as evidenced in the ac shielding data for 1 mT. On the other hand, the damping behavior seems to correlate with the field range of second magnetization peak anomaly. In the measurements at 6.1 K, an obvious second magnetization peak is observed in sample C, while there is no obvious one in sample A.[30] In addition, we have found in sample C that another second magnetization peak appears around 2.5 T in the measurements at a lower temperature of 2.1 K. These observations seem to accord with the fact that the kink structure is very clear in sample C, and its position is approximately the same as that of the second magnetization peak at 2.5 T, while the kink structure of sample A is not very obvious. As mentioned in Sec. I, a disorder in the flux line lattice has been inferred to develop around 2 T in the literature. If the second magnetization peak is somehow related with a disorder, we may assume that the dHvA signal is seriously deteriorated by such a disorder giving rise to the observed damping behavior. Although the pinning effect seems to be negligible under sufficiently large modulation amplitude, we conjecture that a disorder in flux line lattice could remain at low fields. The field strength where a significant disorder starts to develop may increase with the tilting angle from the [001] direction and, consequently, the field at the kink position increases because the transition field from hexagonal lattice to quasisquare one increases as the field orients away from an axis toward the (001) plane. Upon approaching H_{c2}, a homogeneous lattice of possibly hexagonal symmetry with apex angle 60 degrees may recover under the large modulation field, and it may give the lower damping rate.

IV. SUMMARY AND CONCLUSION

We have observed the dHvA oscillations α and η in the mixed state and revealed the anisotropy of the damping behavior due to superconductivity on a single Fermi surface. The anisotropy of the damping rate is consistent with the gap anisotropy probed by other methods if the recent theoretical interpretation of the previous experiment is correct. Moreover, the different damping rate between the Fermi surfaces of α and η suggests that the superconducting gap is different depending on the Fermi surface. On the other hand, the field dependence of the oscillation amplitude in fields far below H_{c2} cannot be understood in terms of the superconducting gap. We suspect that it arises from a disorder of the flux line lattice. The present results indicate that the disorder of the flux line lattice, as well as superconducting gap, is likely to be responsible for the damping of the dHvA oscillations in the mixed state. However, for satisfactory interpretations of the present results further development of the theory for the quantum oscillations in the mixed state, particularly the one which takes the effect of the flux line lattice into account properly, would be necessary.

ACKNOWLEDGMENTS

We are very grateful to P. C. Canfield for permitting us to perform measurements on his very nice crystals of $LuNi_2B_2C$, which was from the same batch as used in an earlier neutron study (Ref. 27). We also acknowledge M. R. Eskildsen for discussions on magnetization data in these crystals. This work was supported by a Grant-in-Aid from MEXT Japan. T. Isshiki acknowledges the support from JSPS.

[1] J. E. Graebner and M. Robbins, Phys. Rev. Lett. **36**, 422 (1976).
[2] N. Doiron-Leyraud, C. Proust, D. LeBoeuf, J. Levallois, J. B. Bonnemaison, R. Liang, D. A. Bonn, W. N. Hardy, and L. Tailefer, Nature (London) **447**, 565 (2007).
[3] S. E. Sebastian, N. Harrison, E. Palm, T. P. Murphy, C. H. Mielke, R. Liang, D. A. Bonn, W. H. Hardy, and G. G. Lonzarich, Nature (London) **454**, 200 (2008).
[4] Y. Inada and Y. Ōnuki, Low Temp. Phys. **25**, 573 (1999).
[5] K. Maki, Phys. Rev. B **44**, 2861 (1991).
[6] K. Miyake, Physica B **186-188**, 115 (1993).
[7] S. Dukan and Z. Tešanović, Phys. Rev. Lett. **74**, 2311 (1995).
[8] M. R. Norman, A. H. MacDonald, and H. Akera, Phys. Rev. B **51**, 5927 (1995).
[9] T. Maniv, V. Zhuravlev, I. Vagner, and P. Wyder, Rev. Mod. Phys. **73**, 867 (2001).
[10] K. Yasui and T. Kita, Phys. Rev. B **66**, 184516 (2002).
[11] E. Steep, S. Rettenberger, F. Meyer, A. G. M. Jansen, W. Joss, W. Biberacher, E. Bucher, and C. S. Oglesby, Physica B **204**, 162 (1995).
[12] R. J. Cava, H. Takagi, H. W. Zandbergen, J. J. Krajewski, W. F. Peck, Jr., T. Siegrist, B. Batlogg, R. B. van Dover, R. J. Felder, K. Mizuhashi, J. O. Lee, H. Eisaki, and S. Uchida, Nature (London) **367**, 252 (1994).
[13] I.-S. Yang, M. V. Klein, S. L. Cooper, P. C. Canfield, B. K. Cho, and S.-I. Lee, Phys. Rev. B **62**, 1291 (2000).
[14] T. Yokoya, T. Kiss, T. Watanabe, S. Shin, M. Nohara, H. Takagi, and T. Oguchi, Phys. Rev. Lett. **85**, 4952 (2000).
[15] K. Izawa, K. Kamata, Y. Nakajima, Y. Matsuda, T. Watanabe, M. Nohara, H. Takagi, P. Thalmeier, and K. Maki, Phys. Rev. Lett. **89**, 137006 (2002).
[16] T. Park, M. B. Salamon, E. M. Choi, H. J. Kim, and S.-I. Lee, Phys. Rev. Lett. **90**, 177001 (2003).
[17] T. Park, E. E. M. Chia, M. B. Salamon, E. D. Bauer, I. Vekhter, J. D. Thompson, E. M. Choi, H. J. Kim, S.-I. Lee, and P. C. Canfield, Phys. Rev. Lett. **92**, 237002 (2004).
[18] S. Mukhopadhyay, G. Sheet, P. Raychaudhuri, and H. Takeya, Phys. Rev. B **72**, 014545 (2005).
[19] C. L. Huang, J.-Y. Lin, C. P. Sun, T. K. Lee, J. D. Kim, E. M. Choi, S. I. Lee, and H. D. Yang, Phys. Rev. B **73**, 012502 (2006).
[20] K. Maki, P. Thalmeier, and H. Won, Phys. Rev. B **65**, 140502(R) (2002).
[21] Q. Yuan and P. Thalmeier, Phys. Rev. B **68**, 174501 (2003).
[22] M. Yethiraj, D. McK. Paul, C. V. Tomy, and E. M. Forgan, Phys. Rev. Lett. **78**, 4849 (1997).
[23] Y. De Wilde, M. Iavarone, U. Welp, V. Metlushko, A. E. Koshelev, I. Aranson, G. W. Crabtree, and P. C. Canfield, Phys. Rev. Lett. **78**, 4273 (1997).
[24] M. R. Eskildsen, P. L. Gammel, B. P. Barber, A. P. Ramirez, D. J. Bishop, N. H. Andersen, K. Mortensen, C. A. Bolle, C. M. Lieber, and P. C. Canfield, Phys. Rev. Lett. **79**, 487 (1997).
[25] H. Sakata, M. Oosawa, K. Matsuba, N. Nishida, H. Takeya, and K. Hirata, Phys. Rev. Lett. **84**, 1583 (2000).
[26] L. Ya. Vinnikov, T. L. Barkov, P. C. Canfield, S. L. Bud'ko, J. E. Ostenson, F. D. Laabs, and V. G. Kogan, Phys. Rev. B **64**, 220508(R) (2001).
[27] M. R. Eskildsen, A. B. Abrahamsen, V. G. Kogan, P. L. Gammel, K. Mortensen, N. H. Andersen, and P. C. Canfield, Phys. Rev. Lett. **86**, 5148 (2001).
[28] T. Park, A. T. Malinowski, M. F. Hundley, J. D. Thompson, Y. Sun, M. B. Salamon, E. M. Choi, H. J. Kim, S. I. Lee, P. C. Canfield, and V. G. Kogan, Phys. Rev. B **71**, 054511 (2005).
[29] D. Jaiswal-Nagar, A. D. Thakur, S. Ramakrishnan, A. K. Grover, D. Pal, and H. Takeya, Phys. Rev. B **74**, 184514 (2006).
[30] D. Jaiswal-Nagar, D. Pal, M. R. Eskildsen, P. C. Canfield, H. Takeya, S. Ramakrishnan, and A. K. Grover, Pramana, J. Phys. **66**, 113 (2006).
[31] M. Heinecke and K. Winzer, Z. Phys. B: Condens. Matter **98**, 147 (1995).
[32] T. Terashima, H. Takeya, S. Uji, K. Kadowaki, and H. Aoki, Solid State Commun. **96**, 459 (1995).
[33] G. Goll, M. Heinecke, A. G. M. Jansen, W. Joss, L. Nguyen, E. Steep, K. Winzer, and P. Wyder, Phys. Rev. B **53**, R8871 (1996).
[34] T. Terashima, C. Haworth, H. Takeya, S. Uji, H. Aoki, and K. Kadowaki, Phys. Rev. B **56**, 5120 (1997).
[35] D. Bintley and P. J. Meeson, Physica C **388-389**, 181 (2003).
[36] O. Ignatchik, T. Coffey, J. Hagel, M. Jäckel, E. Jobiliong, D. Souptel, G. Behr, and J. Wosnitza, J. Magn. Magn. Mater. **290-291**, 424 (2005).
[37] B. Bergk, O. Ignatchik, A. D. Bianchi, M. Jäckel, J. Wosnitza, J. Perenboom, and P. C. Canfield, Physica C **460-462**, 630 (2007).
[38] P. C. Canfield, P. L. Gammel, and D. J. Bishop, Phys. Today **51**(10), 40 (1998), and the references therein.
[39] D. Shoenberg, *Magnetic Oscillations in Metals* (Cambridge University Press, Cambridge, 1984).
[40] M. Endo, N. Kimura, and H. Aoki, J. Phys. Soc. Jpn. **74**, 3295 (2005), and references therein.
[41] T. J. B. M. Janssen, C. Haworth, S. M. Hayden, P. Meeson, M. Springford, and A. Wasserman, Phys. Rev. B **57**, 11698 (1998).
[42] D. Jaiswal-Nagar, Ph.D. thesis, Tata Institute of Fundamental Research, 2007.
[43] M. Tokunaga, N. Miura, H. Takagi, and R. J. Cava, J. Phys. Soc. Jpn. **64**, 1458 (1995).
[44] S. L. Bud'ko, V. G. Kogan, and P. C. Canfield, Phys. Rev. B **64**, 180506(R) (2001).
[45] D. Jaiswal-Nagar, A. D. Thakur, M. R. Eskildsen, P. C. Canfield, S. M. Yusuf, S. Ramakrishnan, and A. K. Grover, Physica B **359-361**, 476 (2005).
[46] S. V. Shulga, S.-L. Drechsler, G. Fuchs, K.-H. Müller, K. Winzer, M. Heinecke, and K. Krug, Phys. Rev. Lett. **80**, 1730 (1998).
[47] G. M. Schmiedeshoff, J. A. Detwiler, W. P. Beyermann, A. H. Lacerda, P. C. Canfield, and J. L. Smith, Phys. Rev. B **63**, 134519 (2001).
[48] E. Wimmer, H. Krakauer, M. Weinert, and A. J. Freeman, Phys. Rev. B **24**, 864 (1981).
[49] T. Siegrist, H. W. Zandbergen, R. J. Cava, J. J. Krajewski, and W. F. Peck, Jr., Nature (London) **367**, 254 (1994).
[50] K. Yamauchi and t H. Harima, Physica B **359-361**, 597 (2005).
[51] K. Yamauchi, H. Katayama-Yoshida, A. Yanase, and H. Harima, Physica C **412-414**, 225 (2004).
[52] B. Bergk, V. Petzold, H. Rosner, S. L. Drechsler, M. Bartkowiak, O. Ignatchik, A. D. Bianchi, I. Sheikin, P. C. Canfield, and J. Wosnitza, Phys. Rev. Lett. **100**, 257004 (2008).
[53] L. H. Nguyen, G. Goll, E. Steep, A. G. M. Jansen, P. Wyder,

O. Jepsen, M. Heinecke, and K. Winzer, J. Low Temp. Phys. **105**, 1653 (1996).
[54] Y. Nagai, Y. Kato, N. Hayashi, K. Yamauchi, and H. Harima, Phys. Rev. B **76**, 214514 (2007).
[55] T. Isshiki, H. Maruyama, N. Kimura, T. Nojima, A. Ochiai, and H. Aoki, Physica C **417**, 110 (2005).
[56] A. Carrington, J. D. Fletcher, and H. Harima, Phys. Rev. B **71**, 174505 (2005).